RSC Publishing Faraday Discussions

Impact of radiation induced crystallization on programmable metallization cell electrical characteristics and reliability

Journal:	*Faraday Discussions*
Manuscript ID	FD-ART-06-2018-000125.R1
Article Type:	Paper
Date Submitted by the Author:	02-Aug-2018
Complete List of Authors:	Gonzalez Velo, Yago; Arizona State University, ECEE Patadia, Arshey; ASU, ECEE Barnaby, Hugh; Arizona State University, ECEE Kozicki, Michael; Arizona State University, Center for Applied Nanoionics

Impact of radiation induced crystallization on programmable metallization cell electrical characteristics and reliability

Yago Gonzalez-Velo, Arshey Patadia, Hugh J. Barnaby, Michael N. Kozicki
School of Electrical, Computer and Energy Engineering, Arizona State University, 650 E Tyler Mall, 85287 Tempe, Arizona, USA

Abstract:

Chalcogenide-based, programmable metallization cells (PMC) cells have been characterized after exposure to increasing levels of absorbed dose (i.e., ionizing radiation exposure). We found, and show here for the first time, that total absorbed dose effects induce a slight modification of the switching phenomena with a moderate increase of the programmable low resistance state (LRS) of the PMCs after repeated switching depending on the processing conditions, while it does not impact the state programmed before exposure. We also show that an increase of the programmable high resistance state (HRS) occurs with irradiation. Such observations are discussed through correlation with crystallization observed in concurrent X-ray diffraction (XRD) characterization of representative thin-film stacks of the PMCs. These new results are compared to previous results obtained on chalcogenide-based PMCs that did not identify/observe such effects.

Submission to the Faraday Discussions

Introduction

Space environment – challenge for electronics. The space environment in which satellites operate is often described as a harsh environment as ionizing radiation exists within the Van Allen radiation belts surrounding the Earth **[1]**, as illustrated in Figure 1 . Electrons and protons trapped in the Earth's magnetic field form those Van Allen belts and can directly impact the operation of microelectronic/nanoelectronic devices. In space systems, effects known as *cumulative effects,* such as total dose effects **[2]** and displacement damage effects **[3],** are related to the trapped electrons and protons in the radiation belts. Other effects, such as single event effects, also occur which are caused by cosmic rays/heavy ions and protons. Single event effects are generally referred to as *transient effects* due to current/voltage transients generated within the devices and collected at a PN junction. *Cumulative effects* are effects that 'accumulate' as a function of time, leading to variations in the microelectronic device's electrical characteristics, including device failure in the worst case. Total dose effects are not only a concern for space microelectronics; microelectronic devices used in medical devices, in industrial systems (nuclear power generation plants and fuel cycle management/storage facilities), or in large high-energy physics (HEP) experiments also suffer from total dose effects in their environment of operation.

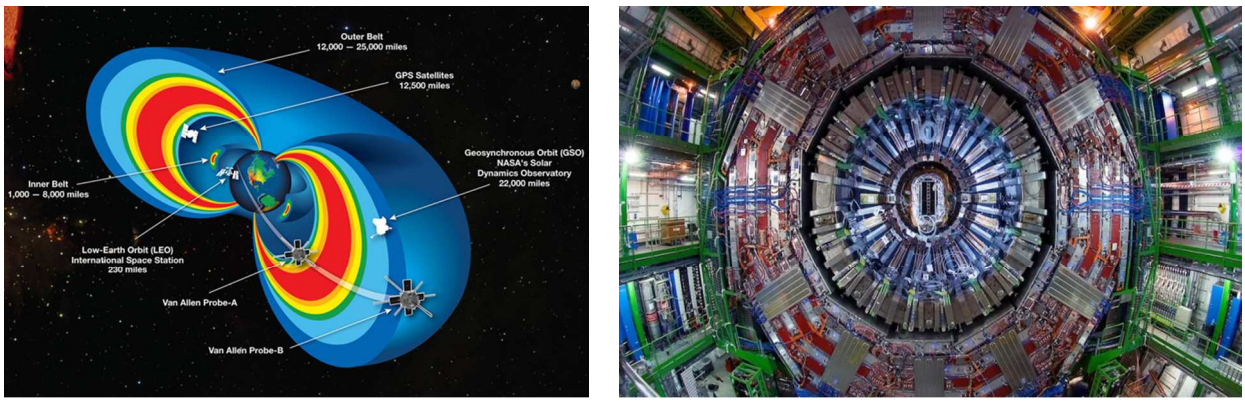

(a) (b)

Figure 1: (a) Illustration of the Van Allen radiation belts surrounding the Earth with the inner belt and outer belt represented and how different orbits might travel through such radiation belts. Image from NASA [**4**], (b) Illustration of the ATLAS detector at CERN, ATLAS and other HEP detectors are made of very large amounts of instrumentation and data processing units. Dose levels over the life of an upgrade /experiment can reach megarads, if not gigarads in the latest LHC upgrade **[5]**.

Resistive RAM (ReRAM) devices have attracted considerable interest and demonstrated a lot of promise for applications in non-volatile memory (NVM) circuits **[6]** as well as, more recently, in applications related to neuromorphic computing **[7]**. The use of ReRAM devices as a solid-state implementation of 'neuron-like' devices has opened the way to the application/use of such devices in artificial intelligence with strong possibilities for reducing the learning time of solid state neuro-computers and providing faster data processing. Space systems or HEP systems deal with extremely large amounts of data with critical/high added value information. Each would benefit from high density, fast NVM memories and novel on-board neuro-processing units with high radiation hardness. In addition, HEP or industrial applications would benefit from low-to-medium density rad-hard NVM memory with very low power consumption that could be implemented in IoT monitors/sensors of the facilities.

The understanding of ionizing radiation effects on ReRAM devices in general suffers from the fact that resistive switching has been observed and presented in so many different materials **[8]**

in the last few years – with no clear material system prevailing and with myriad different mechanisms possible – which also limits the knowledge and analysis available on such reliability effects. Nevertheless, the data collected by different groups on different NVM ReRAM technologies seems to show that such devices exhibit high/very high levels of radiation hardness, making them extremely good candidates for radiation-hard NVM. However, less is known about the analog operation of such devices after exposure to ionizing radiation.

In this work, we focus on total dose effects on the resistance/resistive switching of programmable metallization cell (or conductive-bridging RAM CBRAM, or electro-metallization cell EMC) devices. Chalcogenide-based PMC/CBRAM is the main focus of this work, however reference will be made to oxide-based CBRAM, and, when appropriate, to oxide-RAM (OxRAM), device observations. In the Experimental Protocol section, the different manufacturing, electrical characterization and material characterization techniques and procedures are described. In the Experimental Results and Analysis sections, the data obtained are carefully presented and reviewed. Lastly, a discussion is provided related to effects and analysis that have been observed by several other teams of researchers who focus on total dose effects on ReRAM devices.

1. Experimental protocol

A. Ionizing radiation exposure

Total dose (TID) effects are commonly investigated by using cobalt-60 gamma-ray irradiators to irradiate microelectronic devices/circuits. Cobalt-60 (Co-60) gamma-ray exposure is the standard method **[9]** for TID testing conducted by space agencies and the space/defense industry for flight lot qualification or to investigate dose effects on novel technologies. TID effects induced by Co-60 gamma-rays have been shown to accurately reproduce the degradations observed on different microcircuits on board satellites, i.e., reproduce the effects of the environment created by electrons and protons from the Van Allen belts.

The high-energy photons produced by the radioactive decay of Co-60 enable us to reach electronic equilibrium conditions **[10]** and avoid dose reinforcement issues encountered with X-ray exposures at the interface between high-Z and low-Z material. Such ionizing radiation enables generation of electron/hole pairs (ehp) within the materials constituting the devices (and maybe also electron/cation or hole/anion pairs in the case of ReRAM materials).

For space applications, depending on the mission (i.e., duration, flight orbit, etc.) the TID seen by a microelectronic circuit can range from a couple of tens of kilorad to several megarad. The highest TIDs are generally known to be present in very challenging research missions around Jupiter and its moons, or necessary to qualify some defense systems **[11]**. In the case of HEP experiments, multi-megarad doses are very common over the life of a system between upgrades **[12].**

The Co-60 irradiator used in this work is a Gammacell 220 available at the radiation damage laboratory at Arizona State University. The samples were placed in the irradiator without bias (i.e., left floating). The dose-rate of the exposure was 271 rad($Ge_{30}Se_{70}$)/s (i.e., 2.71 Gy/s, with Gray (Gy) the S.I. unit corresponding to 1 J / kg = 100 rad of absorbed energy per kg of mass).

B. PMC description - Processing description

The CBRAM cells used were manufactured in the ASU Nanofab clean-room facility on the Arizona State University campus. The fabrication process began with the deposition of the bottom electrode which was an 80 nm blanket film of DC-sputtered tungsten. An isolation

dielectric is then deposited by PE-CVD to enable the via formation in which the PMC is created. The solid-state electrolyte in which resistive switching occurs is formed by thermal evaporation conducted in a Cressington 308 system, with the evaporation source being $Ge_{30}Se_{70}$ chalcogenide glass (ChG). 60 nm of $Ge_{30}Se_{70}$ was deposited on the substrates and an additional 30 nm of Ag was deposited on top of the ChG without breaking the vacuum of the thermal evaporator, with pressure kept at levels lower than 10^{-6} mbar, and deposition rates not in excess of 0.1 nm/s. UV-light exposure was then conducted on the 30 nm Ag / 60nm $Ge_{30}Se_{70}$ stack to induce photodoping of Ag and once the photodoping step was finalized, an additional 30 nm of Ag was deposited to obtain a continuous top Ag electrode. The last step of processing consisted of the patterning of a 300 nm Al top contact deposited by electron-beam evaporation. These devices are briefly illustrated in Figure 2 with their top view and their cross-section description provided. The results presented were obtained on PMCs with a 5 µm diameter.

Once manufactured, one set of devices (all devices came from the same wafer) was subjected to an 80°C annealing for 60 minutes, whereas the other set of devices was not submitted to any post manufacturing annealing. This constitutes two sets of devices that are investigated in this work with the goal of observing manufacturing process related differences in the response/behavior of the devices. In addition to the PMC manufactured as resistance switching elements, PMC stacks of blanket thin-films were also manufactured to enable characterization of the films. The annealing was conducted since in a previous work it was obtained that radiation hardening by process (i.e. improving the total dose response by a manufacturing process modification) was achievable through post manufacturing annealing **[13]**.

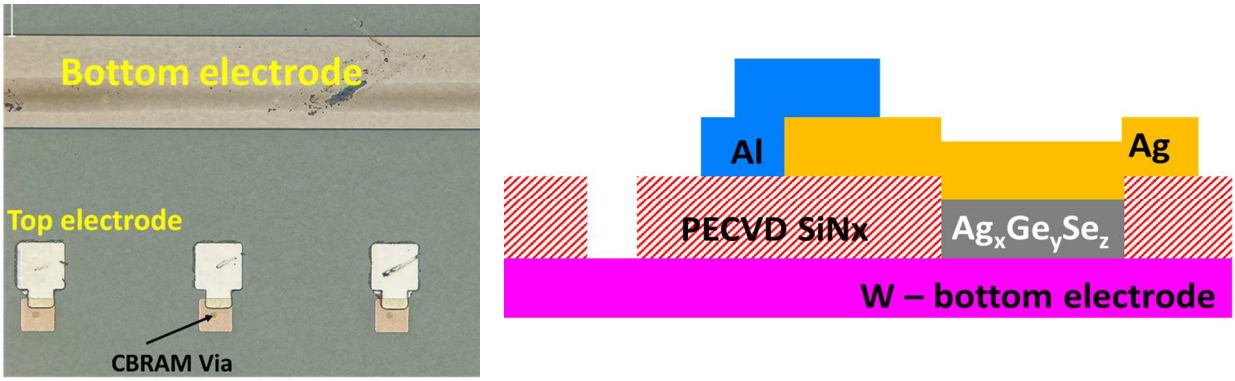

(a) (b)

Figure 2: (a) Top view of PMC devices with the access to bottom electrode, top electrode bond-pad and PMC/CBRAM via illustrated; (b) cross section of the PMC/CBRAM devices studied in this work.

The yield of the PMCs manufactured was very high. 100% of the devices tested were operational, the only yield issue being related to the lift-off of the top Al contact which leaves some of the PMC without a top Al contact. Such devices without top Al contact were not tested.

C. Electrical characterization description

The 2 batches of PMC devices (annealed and not annealed) were exposed to Co-60 gamma-rays, with devices being DC-IV switched before and after exposure to observe the impact of TID on the resistive switching capability and properties of the cells. CBRAM cells were exposed in their ON-state (or LRS state), as well as in a 'non-formed' (never switched) state. Repeated IV characteristics were obtained before and after irradiation and typical parameters of R_{on} (LRS), R_{off} (HRS), V_{set} (or V_{prog}) and V_{erase} (or V_{reset}) were extracted. The devices were characterized by

DC-IV switching with the same DC-IV set-up, an Agilent 4156C semiconductor parameter, and a fixed programming current (compliance current) of 10 microamperes. Care was taken to compare data obtained under similar DC-IV conditions (same number of steps, same integration times, same SMU resolution setting, etc.) to avoid effects related to variation in voltage ramp speed.

The V_{set} presented in this work were extracted as the point at which the derivative dI / dV is maximal, and R_{on} and R_{off} values are presented as the resistance on the IV characteristic measured at an applied voltage of 30 mV. V_{erase} is extracted as the voltage at which the minimal value of current occurs in a range of voltages known to be the range in which erase occurs. Nevertheless, such extraction has its own limitation, which will be described once the cumulative distribution function (CDF) of V_{erase} are presented.

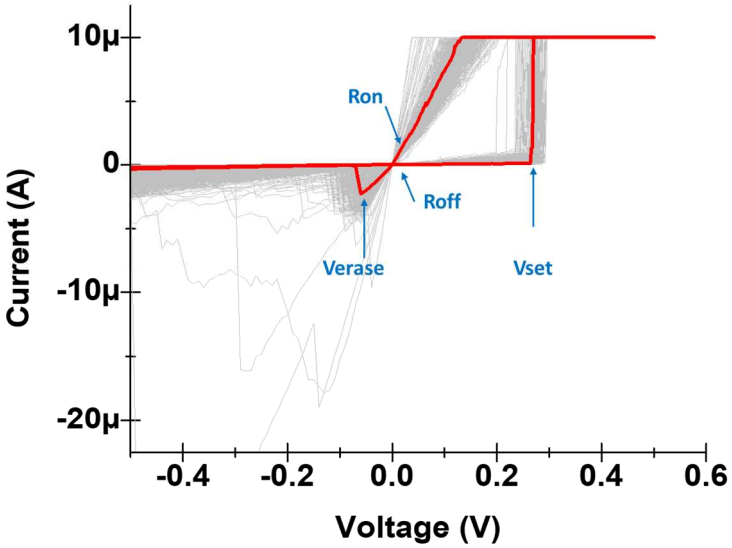

Figure 3: Typical set of DC-IV characteristic used to extract R_{on}, R_{off}, V_{erase} and V_{set}. In this case, 500 DC-IV switching are conducted with a programming current of 10 µA. In red, one of the DC-IV curves is highlighted to illustrate the typical values extracted.

D. X-ray diffraction characterization

X-ray diffraction was conducted at the Eyring Material Center at ASU. A Bruker D8 diffractometer with a beam mask and a Gobel mirror was used, having a Cu filament operated at 40 kV and 40 mA. The mode of operation utilized was '*detector scan*' with a glancing angle of 1 degree selected after glancing angle optimization. The scans were conducted for 2 θ angles ranging from 10 degrees to 85 degrees with a step of 0.047 degree.

2. Experimental results and analysis

Resistive switching behavior - Typical DC-IV switching was conducted on the two different sets of devices (annealed and non-annealed), on devices not exposed to radiation (control devices), and devices exposed to increasing TID values (different sets *rad1*: 1.06 Mrad and *rad2*: 2.38 Mrad). Cumulative density function (CDF) plots obtained after 500 repeated resistance switching operations on 3 devices of each type are presented in Figure 4 through Figure 8. V_{set} was obtained on voltage sweeps conducted with a voltage step of 2 mV from 0 V to 0.5 V in order to provide a +/- 2 mV resolution on the V_{set} characterization. The reset/erase operation was conducted with a voltage step of 10 mV from 0 V to -1 V, which exhibits larger

'staircase' steps on the different CDF reported for $V_{erase.}$ In Figure 4, a brief comparison is provided between the DC extracted parameters for the devices undergoing the one hour 80°C annealing (black, open square symbols) and devices not undergoing such annealing (blue, downward open triangles).

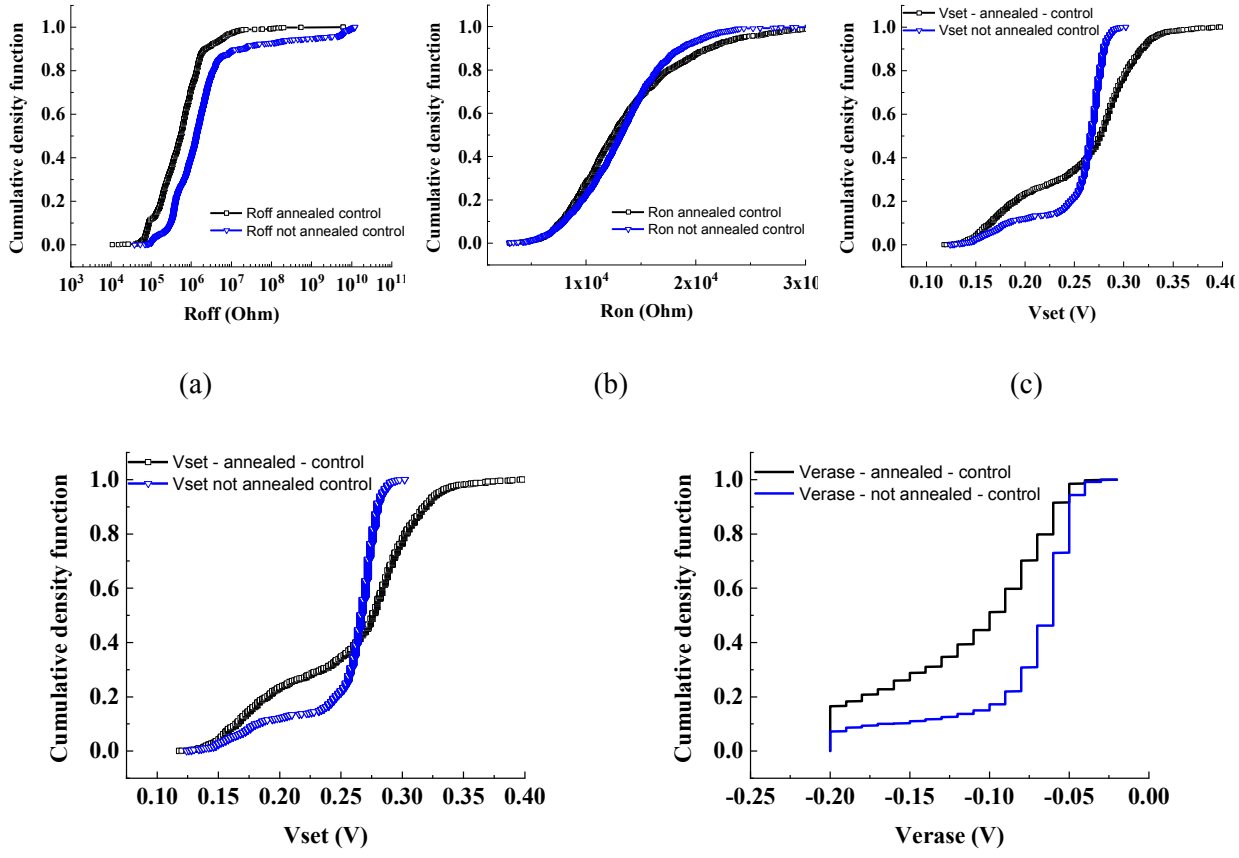

Figure 4: CDF plots of (a) R_{off}; (b) R_{on}, (c) Ratio of R_{off}/R_{on} , (d) V_{set} and (e) V_{erase} for the 500 first resistance switching operations for 3 different devices from each processing batch (annealed and not annealed).

We found that the HRS state (R_{off}) of the annealed samples shifted towards lower resistance values when compared to non-annealed samples. However, the LRS state values obtained are very similar for both annealed and non-annealed samples. Since the LRS resistance values are similar, the R_{off}/R_{on} ratio trend is in-turn similar to the HRS. Moreover, the R_{off}/R_{on} was smaller for annealed samples compared to non-annealed samples. The set and erase also exhibited some differences from one process batch to another; the V_{set} and V_{erase} had tighter distributions for the case of the non-annealed batch. V_{set} and V_{erase} also tended to have lower values in the non-annealed batch.

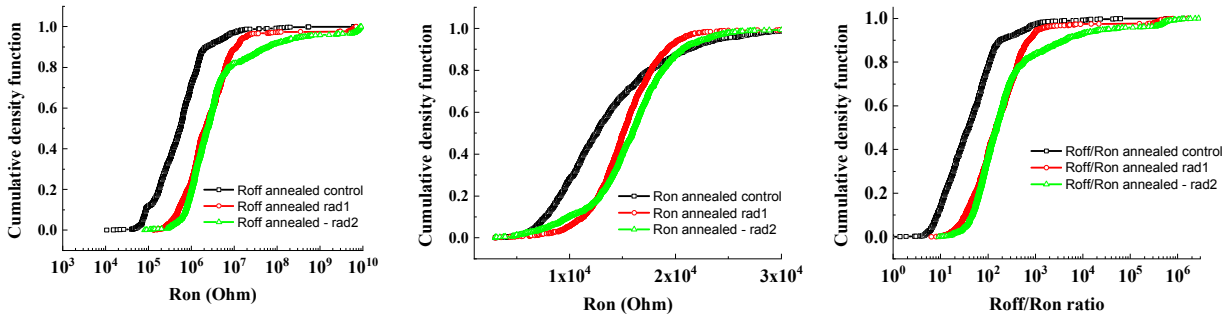

(a) (b) (c)

Figure 5: CDF plots of (a) R_{off}; (b) R_{on}, (c) Ratio of R_{off}/R_{on} for the 500 first resistance-switching operations of different sets of 3 annealed devices exposed to increasing steps of total dose.

The DC-IV extracted characteristics for annealed devices exposed to ionizing radiation are shown in Figure 5. We observed that for annealed samples, an increase of R_{off} and R_{on} occurs, with wider distributions of the resistance value. This was the first time that such monotonic increase of R_{on} was observed on such PMCs.

The results from non-annealed devices are slightly different and are illustrated in Figure 6. It can be observed that a non-monotonic behavior occurs with TID, with first an increase of HRS and LRS occurring up to 1.06 Mrad, whereas a decrease of both R_{off} and R_{on} then occurs at 2.38 Mrad.

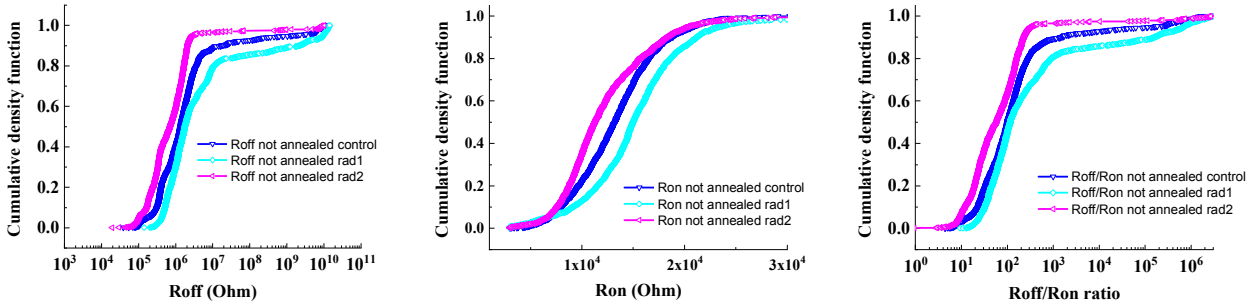

(a) (b) (c)

Figure 6: CDF plots of (a) R_{off}; (b) R_{on}, (c) Ratio of R_{off}/R_{on} for the 500 first resistance-switching operations of different sets of 3 non-annealed devices exposed to increasing steps of total dose

V_{set} distributions for both types of samples reveals a slight impact of total dose based upon the way these devices are set. For annealed device and non-annealed devices, it is observed for non-exposed devices that V_{set} distributions occur around "preferred values" of 160 mV and 260 mV, with 260 mV being the most common. In the case of annealed samples, a minimal variation of V_{set} distribution is observed after 1.06 Mrad, and V_{set} tends to decrease for additional TID. In the case of the annealed samples, V_{set} shows an important tightening of the distribution with a slight decrease of the V_{set} maximal values and a decrease of the occurrences of lower V_{set} values.

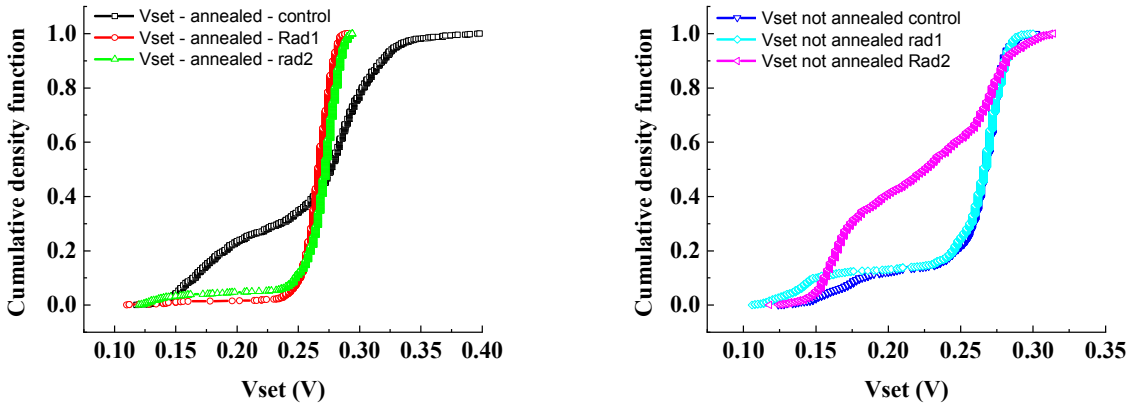

(a) (b)

Figure 7: CDF plots of (a) V_{set} for devices from both processing batches not exposed to ionizing radiation; (b) V_{set} for annealed devices exposed to ionizing radiation; (c) V_{set} for non-annealed devices exposed to ionizing radiation

V_{erase} distributions are presented in Figure 8. The V_{erase} extracted on erase sweeps were conducted with step sizes of 10 mV. This impacted the resolution of the distribution, but the obtained results still provide interesting insight into how erase occurs at lower voltage with TID for annealed devices and V_{erase} increases for annealed devices. Consequently, it is easier to erase annealed devices after exposure and harder to erase non-annealed devices. (*The terms increase and decrease are used literally here with respect to the abscissa of the figures, i.e. -1 V is lower than -0.5 V*)

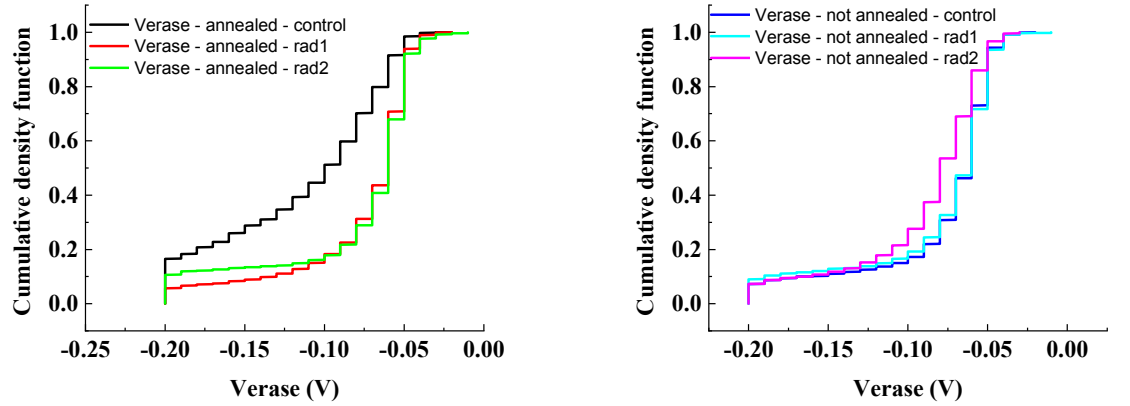

(a) (b)

Figure 8: CDF plots of (a) V_{erase} for devices from both processing batches not exposed to ionizing radiation; (b) V_{erase} for annealed devices exposed to ionizing radiation; (c) V_{erase} for non-annealed devices exposed to ionizing radiation

ON state retention – Devices were exposed in their ON-state to observe the impact of total dose on LRS retention. The IV erasing sweeps of the devices are shown (in Figure 9) after TID exposure illustrating that devices were still in their ON-state after exposure.

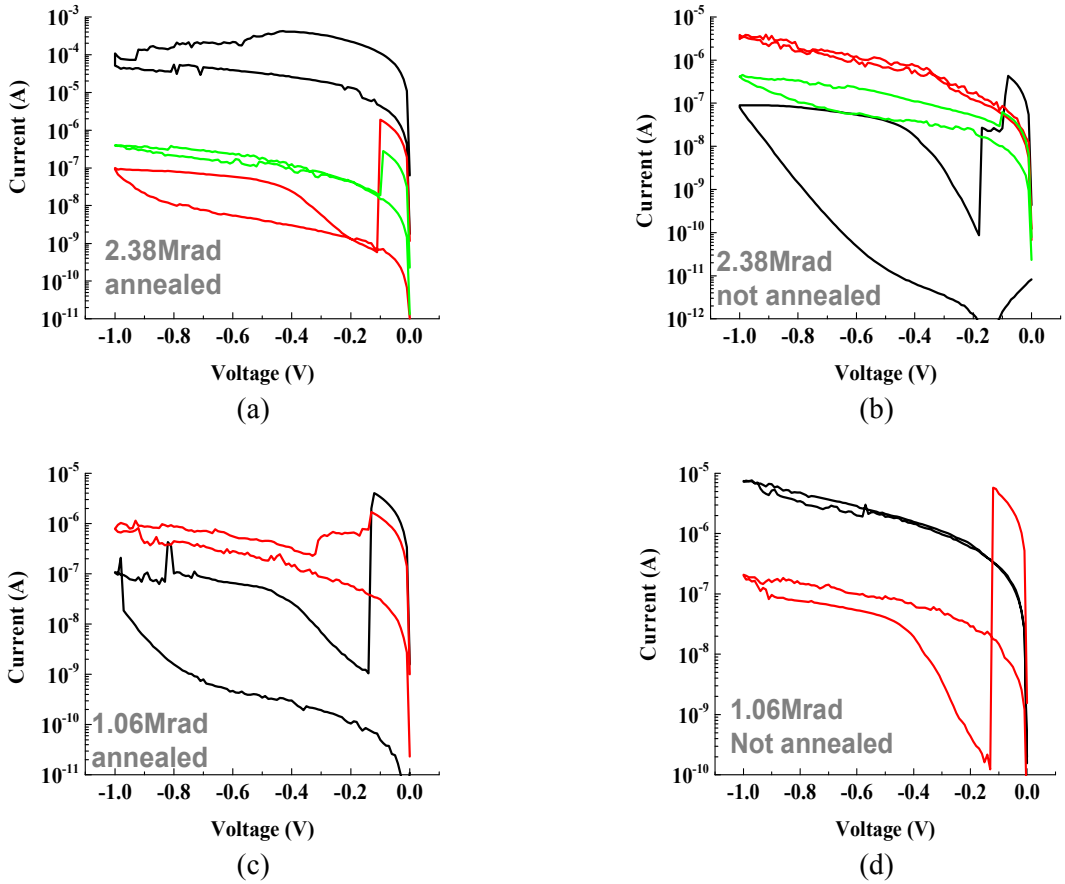

Figure 9: Erase voltage sweeps conducted on samples exposed to ionizing irradiation in their ON-sate (a) 3 annealed devices at 2.38 Mrad, (b) 3 non-annealed devices at 2.38 Mrad, (c) 2 annealed devices at 1.06 MRad, (d) 2 non-annealed devices at 1.06 Mrad.

It was observed that the devices maintained their LRS after exposure. In the case of two devices from the non-annealed samples (one at 1.06 Mrad and another at 2.38 Mrad), the LRS state itself is not erased since the devices exhibit what would be a low resistance of their HRS. This is something that would certainly necessitate additional device testing to provide better statistical representativity.

Forming current – Forming currents measured on the annealed and non-annealed samples are illustrated in Figure 10. Both forming currents are very similar with a slight decrease of current observed on the annealed samples. On samples exposed to ionizing radiation, we observed in the case of the non-annealed samples, a decrease of forming current occurs with total dose (see Figure 10.b) and an increase in current is seen on annealed samples (see Figure 10.c). Nevertheless, such current differences are very minimal and could also be related to the device to device mismatch across the wafer, including thickness non-uniformities existing across the devices.

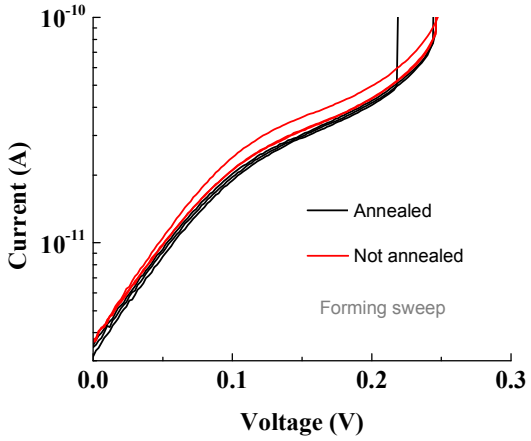

(a)

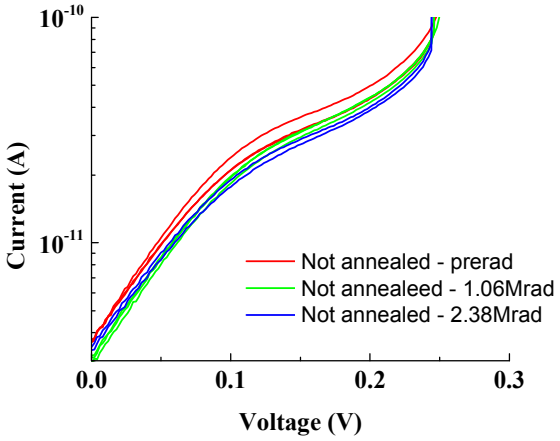

(b)

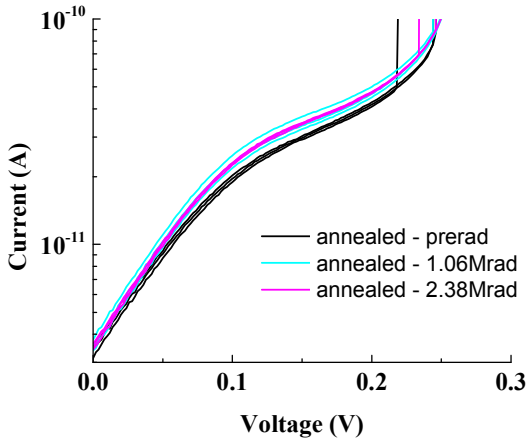

(c)

Figure 10: Forming sweep on samples (a) annealed and non-annealed (b) non-annealed samples before and after total dose exposure, (c) non-annealed samples before and after total dose exposure, voltage is swept with a voltage step of 2 mV

X-ray diffraction characterization – X-ray diffraction was conducted on representative PMC stacks to observe crystallization that could be occurring in the samples. Such crystallization studies have been presented in the literature **[14]** - **[18]** to investigate the impact of temperature budget during processing as well as more recently to investigate the impact of total dose **[16]**, **[18]**. Nevertheless, those XRD studies were conducted on chalcogenide films or chalcogenide-based films with a top layer of silver. In this work, we conducted such characterization on blanket films arrangements representative of the PMC, i.e., with bottom metal (tungsten) and a top layer of silver deposited after a first silver layer is photodoped. Such stacks constitutes a slight challenge since large peaks associated with the polycrystalline bottom and top metal are expected. Nevertheless, metallic filament formation in silver/chalcogenide films is generally associated with the presence of an electric field, and the presence of the bottom tungsten and top silver would help mimic conditions encountered in PMC devices with the impact of the difference of work-function of the metals taking effects in such samples.

The diffractograms obtained are illustrated in Figure 11 and Figure 12 with the number of counts plotted as a function of 2-θ angle. The MDI Jade software and ICDD PDF-4 database were used for data analysis and phase identification.

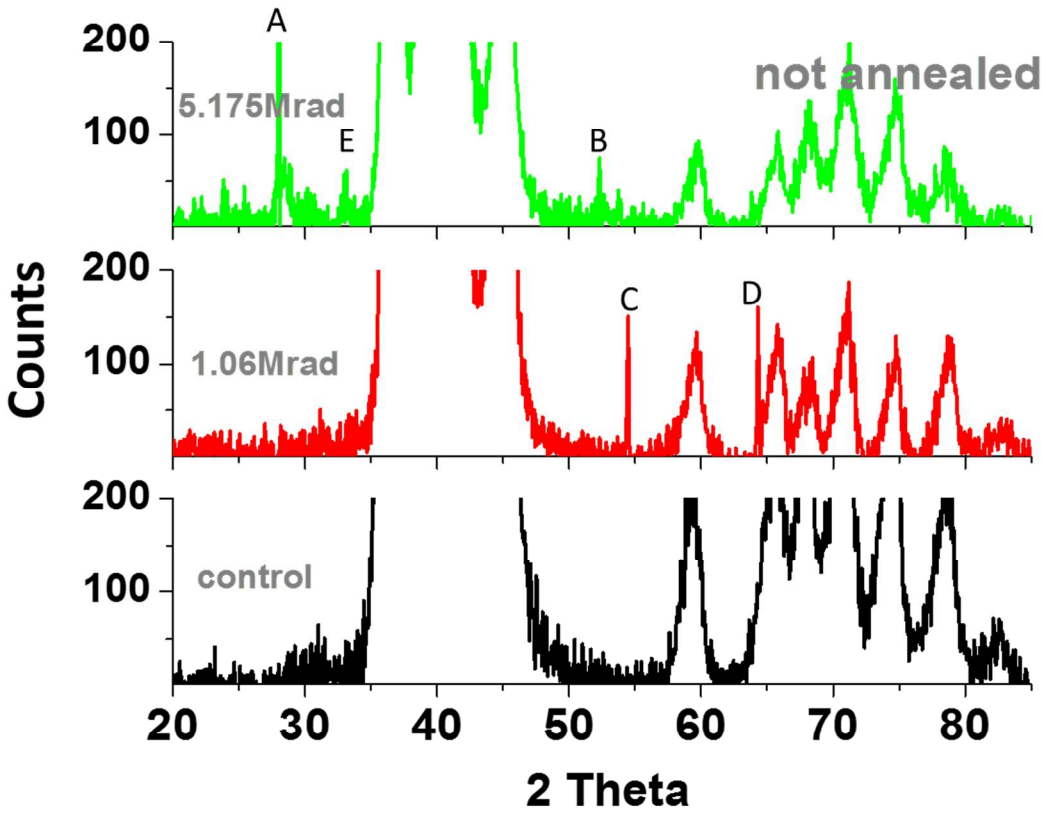

Figure 11: XRD diffractograms obtained on the non-annealed sets of blanket films for films exposed and non-exposed to ionizing radiation

We found that both control samples exhibited very similar diffractograms. From annealed to non-annealed samples, the only difference is the 80-degree Celsius annealing, which might cause some initial crystallites to appear. Such crystallites could be hidden by the large peaks existing between 2-θ values of 40 to 50 degrees. Nevertheless, Bruchaus et al. [14] have shown that for 80°C Ag-GeSe films do not exhibit major/noticeable crystallization on thin-films without a bottom metal layer. It is shown in Figure 11, that several phases appear during exposure to ionizing radiation on non-annealed samples with both Ag_2Se and Ag_8GeSe_6. For such non-annealed samples, Ag_2Se is shown to appear on the samples through peaks labeled D and E (pdf card 01-071-2410), whereas such peaks disappear at higher total dose and leave room to peaks A, B and C, where peak A can be matched to Ag_8GeSe_6 (pdf card 04-008-7238) and peak B corresponds to Ag_2Se (pdf card 00-025-0766).

In the case of the annealed samples, the evolution is found to be quite different than the one observed in the case of non-annealed samples. In this case, no crystallites seem to appear at TID in the range of 1 Mrad, but at TID of 5 Mrad Ag_8GeSe_6 (peak F on Figure 12, pdf card 01-081-2588) appeared on the films.

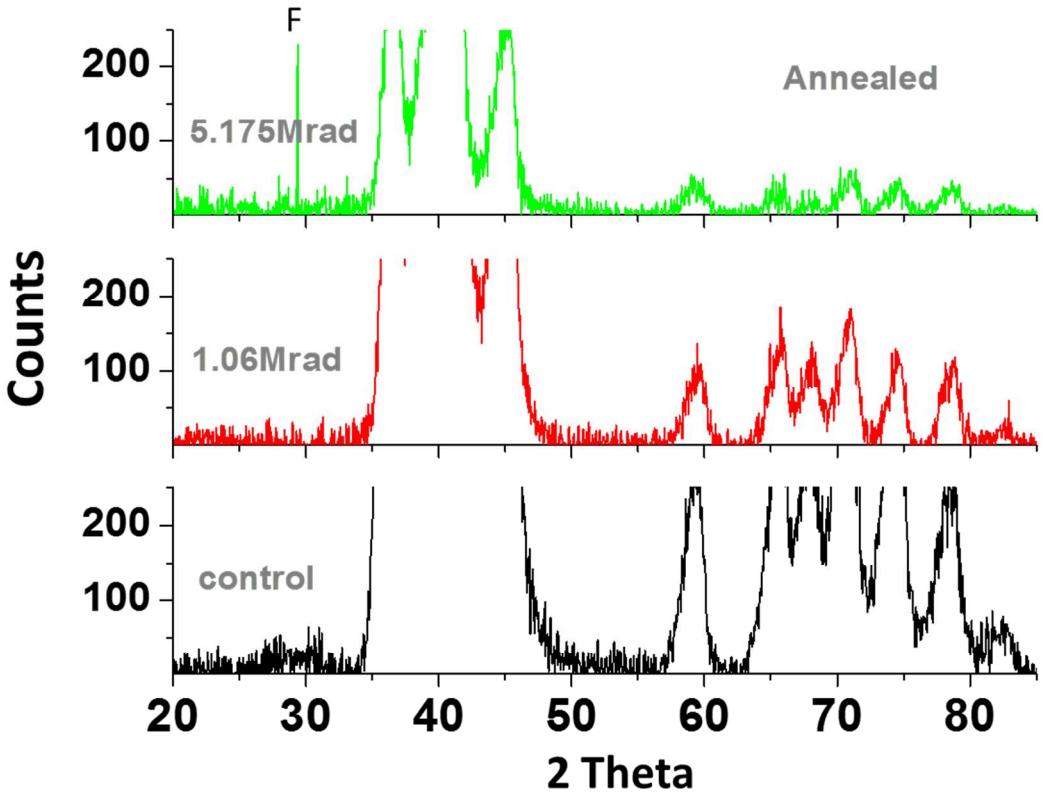

Figure 12: XRD diffractograms obtained on the annealed sets of blanket films for films exposed and non-exposed to ionizing radiation

Discussion

We investigated crystallization effects occurring on blanket films in parallel with the evolution of electrical characteristics of PMCs with TID, with the goal of investigating the root-causes for electrical parameter variation as well as radiation hardening by process.

It is worth mentioning that the DC-IV testing parameter of maximal current allowed to flow through the device (i.e. compliance current or programming current) was kept low in order to minimize silver movement through the films. Large number of resistance switching operations were performed to get a representative behavior. In previous work, high compliance currents were used as well as lower numbers of resistance switching operations which contributed to a reduced characterization of the effects **[13]**, **[19]**.

Even though minimal differences were found on the XRD diffractograms and R_{on} CDF for both non-irradiated annealed and non-annealed samples, differences occur with V_{set} and R_{off}. This illustrated that changes existed between the two fabricated solid-electrolytes that were not observed through XRD. As mentioned, the lack of difference between the diffractograms of control samples might be due to the presence of the large peaks for Ag and W present at angle around 30-40 degrees. However, differences appear with TID as crystallite formation occurs. For annealed samples, it seems that Ag_8GeSe_6 develops preferentially, whereas for non-annealed samples several phases appear, and the onset of crystallite formation occurs at lower TIDs. On the annealed samples, increase of R_{on} could be related to Ag_8GeSe_6 formation which ties Ag into such crystallites and does not contribute as a silver source enabling an increase of HRS and LRS

resistance. In the case of the non-annealed samples, both Ag_2Se and Ag_8GeSe_6 appeared on the samples with different crystallite dimensions revealed by the peak broadening. The existence of such two phases might be related to the non-monotonic behavior observed on the irradiated samples: appearance of phases with different gaps, resistivity and dimensions could impact the R_{on} and R_{off} of the PMCs. Such non-monotonicity has been observed by other investigators [16]. In addition, since both phases have different gaps ($E_g(Ag_2Se)$ = 0.15 eV, density = 8.216 g/cm^2 and $E_g(Ag_8GeSe_6)$ = 0.84-0.88 eV and density around 6.3 g/cm^2), the generation of electron-hole pairs would occur at higher rates than in an impoverished chalcogenide part of the films, making the modeling and understanding of the mechanisms within the different film processing more complex. The resistance switching phenomena is shown not to be removed by TID but some of its characteristics were shown to vary and temperature annealing is shown to provide films/electrolyte that once subjected to TID exhibit a more uniform and improved resistance switching phenomenon (for annealed samples tighter distribution of R_{off}, and V_{set}, reduced V_{erase}).

The on-state retention investigated in this work shows that small filaments (i.e., written with low compliance current) are not impacted by TID and that any modification occurring within the electrolyte in the ON-state does not prevent it from being erased/reset. The forming currents measured before and after exposure are very low and even though a small variation is observed in these currents, such variation could be related to thickness variability within the samples.

Concerning the XRD, additional work will be conducted to estimate the dimensions of the crystallites in order to assess the dimension compared to the thickness of the films and how such dimensions could impact the forming current.

Acknowledgements

The use of facilities within the ASU NanoFab at Arizona State University is acknowledged. The use of facilities within the Eyring Materials Center at Arizona State University is also acknowledged, in particular Dr. Thomas Groy for the help and discussion on the Bruker D8 set-up and XRD diffractograms analysis.

References

[1] J. A. Van Allen, L. A. Frank, “Radiation Around the Earth To a Radial Distance of 107,400 km”, Nature, 1959, doi: 10.1038/1834430a0

[2] H. Barnaby, Total-Ionizing-Dose Effects in Modern CMOS Technologies, *IEEE Trans. on Nuclear Sciences*, pp. 3103-3121, Vol. 53, no. 6, Dec. 2006

[3] J. R. Srour, C. J. Marshall, P. W. Marshall, “Review of Displacement Damage Effects in Silicon Devices,” *IEEE Trans. on Nuclear Sciences*, vol. 50, no. 3, pp. 653-670, June 2003

[4] Van Allen radiation belts with satellites, available Online, June 1st 2018: https://www.nasa.gov/mission_pages/sunearth/news/gallery/20130228-radiationbelts.html

[5] CERN LHC atlas, available online June 2nd 2018: https://home.cern/about/experiments/atlas

[6] Resistive Switching: From Fundamentals of Nanoionic Redox Processes to Memristive Device Applications, Editors(s): Daniele Ielmini, Rainer Waser, Wiley-VCH Verlag GmbH & Co. KGaA, ISBN:9783527334179

[7] G. W. Burr, R. M. Shelby, A. Sebastian, S. Kim, S. Kim, S. Sidler, K.Virwani, M. Ishii, P. Narayanan, A. Fumarola, L. L. Sanches, I. Boybat, M. Le Gallo, K. Moon, J. Woo, H. Hwang,

Y. Leblebici, "Neuromorphic computing using non-volatile memory," Advances in Physics X, Volume 2, 2017 - Issue 1, Pages 89-124
[8] Michael N Kozicki1 and Hugh J Barnaby, Conductive bridging random access memory—materials, devices and applications, Semiconductor Science and Technology, Volume 31, Number 11, October 2016, IOP
[9] Mil-std 883, TM 1019.8 Ionizing radiation (total dose) test procedure. Available online
[10] R. D. Evans, The atomic nucleus, McGraw Hill Inc, 1955
[11] C. Paranicas, J. F. Cooper, H. B. Garrett, R. E. Johnson, J. Sturner,, Europa's Radiation Environment and Its Effects on the Surface,
[12] Burkhard Schmidt, "The High-Luminosity upgrade of the LHC: Physics and Technology Challenges for the Accelerator and the Experiments ", 2016 J. Phys.: Conf. Ser. 706 022002
[13] Y. Gonzalez-Velo, A. Mahmud, W. Chen, J. Taggart, H. Barnaby, M. N. Kozicki, M. Ailavajhala, K. Holbert, M. Mitkova, "Radiation hardening by process of CBRAM resistance switching cells," *IEEE Trans. Nucl. Sci.* vol. **63** pp. 2145–51, 2016
[14] R. Bruchhaus, M. Honalb, R. Symanczyk, M. Kund, "Selection of Optimized Materials for CBRAM Based on HT-XRD and Electrical Test Results," J. Electrochem. Soc. 2009 volume 156, issue 9, H729-H733, doi 10.1149/1.3160570
[15] M. Balakrishnan, M. N. Kozicki, C. D. Poweleit, S. Bhagat, T. L. Alford, M. Mitkova, "Crystallization effects in annealed thin GeS2 films photodiffused with Ag," *Journal of Non-Crystalline Solids*, Volume 353, Issues 13–15, 2007, Pages 1454-1459, ISSN 0022-3093, https://doi.org/10.1016/j.jnoncrysol.2006.09.071.
[16] M. Mitkova, K. Wolf, G. Belev, M. Ailavajhala, D. A. Tenne, H. Barnaby, M. N. Kozicki, "X-ray radiation induced effects in selected chalcogenide glasses and CBRAM devices based on them," *Phys. Status Solidi B*, 253: 1060-1068, (2016), doi:10.1002/pssb.201552562
[17] M.N Kozicki, M Mitkova, J Zhu, M Park, Nanoscale phase separation in Ag–Ge–Se glasses, *Microelectronic Engineering*, Volume 63, Issues 1–3, 2002, Pages 155-159, ISSN 0167-9317, https://doi.org/10.1016/S0167-9317(02)00631-7.
[18] M. S. Ailavajhala, Y. Gonzalez-Velo, C. Poweleit, H. Barnaby, M. N. Kozicki, K. Holbert, D. P. Butt, M. Mitkova, "Gamma radiation induced effects in floppy and rigid Ge-containing chalcogenide thin films," *Journal of Applied Physics,* 115, 043502 (2014); https://doi.org/10.1063/1.4862561
[19] Y. Gonzalez-Velo *et al* , "Total-ionizing dose effects on the resistance switching characteristics of chalcogenide programmable metallization cells," *IEEE Trans. Nucl. Sci.* vol. **60** pp. 4563–9, 2013